Chapter 11 -- Power and Particle Handling and First Wall

11.1 Introduction and General Considerations

Experimental evidence clearly demonstrates that control of neutrals- and impurity influx is a prerequisite for enhanced plasma performance. Accordingly, the goal of the "power- and particle handling" program is to implement heat removal and particle- and impurity control consistent with enhanced plasma performance. This can be accomplished through careful design of the plasma-facing components (PFCs) and optimized plasma operation. The plasma-facing components which intercept particle- and power fluxes need to be capable of accommodating these fluxes without deleterious recycling or impurity production.

Due to their three-dimensional topology, stellarators don't necessarily have the ordered magnetic field line structure outside the separatrix found in axisymmetric tokamaks. Hence, optimized plasma-facing components also must be three-dimensional. Depending on the configuration, they can function as limiters or divertors. In a magnetic configuration with a separatrix, we define the plasma-facing component to be a "limiter" if it is located inside the last closed magnetic surface (LCMS) and intercepts closed field lines, thereby defining the plasma boundary. The same PFC can be a "divertor plate" if it is outside the LCMS and intercepts open field lines only. A fixed set of PFCs can function as a divertor or limiter by magnetically changing the configuration.

A limiter has the advantage of defining the last closed surface and can thus simplify the boundary structure by cutting off islands and ergodic regions, but the disadvantage is that it is in direct contact with the confined plasma and that it can be a strong source of recycling neutrals and impurities. A divertor, on the other hand, provides the advantage of an interface between the plasma and the solid wall which is removed from the confined plasma and buffered by the divertor plasma. However, in a stellarator, the boundary of the main plasma can be very complex, with islands and ergodic regions with short connection lengths which can themselves interact locally with the walls. Therefore, limiter operation may be more easily controllable for initial plasma operation.

With this preamble, we can state that the PFC design in NCSX is carried out with the goal to minimize the impact on plasma performance in the following sense: 1). Heat removal has to be accomplished in a way which avoids excess temperatures on the material surfaces. 2) Neutrals from recycling have to be controlled internally (baffles) and/or externally (pumps) for minimum effect on plasma performance. 3) The plasma-surface interaction has to be designed for minimum impurity generation.

The most basic task of the boundary program is the study of the field line structure outside the LCMS. This is the basis for the design of limiter- or divertor plates and, to some degree, the vacuum vessel. In a modular stellarator, such as NCSX, the plasma configuration outside the separatrix can be very complicated and detailed studies are needed, supported by modeling and experiment, before the optimum divertor can be designed. Some of the basic features can be adopted from the experience of W7-AS and the design studies for W7-X. The Wendelstein group has studied an approach for a stellarator divertor for more than a decade [1] and has developed modeling tools [2] as well as carried out divertor experiments [3]. The final phase of the Wendelstein divertor development is an island divertor in which the islands outside the LCMS are intercepted by divertor plates (open field lines) and the particles are pumped by cryo-pumps located behind baffles. Although the NCSX configuration is different from the Wendelstein configuration, there are indications that field lines outside the LCMS accumulate in the top and bottom of the bean-shaped cross sections and divertor baffles should be effective for neutrals control in these locations.

Since more modeling work and experimental experience is necessary before the ultimate divertor can be designed, we plan a phased approach for the NCSX boundary and divertor development. In the first phase the emphasis is on flexibility to accomodate different plasma configurations and this initial phase might not be optimal concerning all required functions. Adequate power handling, of course, is a prerequisite. The subsequent development will be based on further modeling, experimental feed back and model validation and will eventual lead to the final version combining optimized heat removal with good neutrals- and impurity control.

11.2 Magnetic Topology Outside the Last Closed Magnetic Surface

As indicated above, stellarators are generally thought to lack the ordered magnetic field line structure found in the scrape-off layer of axisymmetric devices. For the quasi- axisymmetric (QAS) stellarator, a tokamak-like ordering becomes evident when the first toroidal intersections of field lines with external walls are abstracted from the more numerous Poincare punctures of a given poloidal plane occuring during multiple transits of the field line around the torus. The intersection with walls limits the stochastic build up in the field line structure that would otherwise accumulate over many toroidal transits of the line. In addition, the existence of an ordered structure of external field lines launched close to the last closed magnetic surface is further revealed by applying the healing technique of Chapter 4 to any island chains just within the LCMS. For practical reasons, individual features of this boundary layer need to be considered for vacuum vessel and PFC design, with the goals of small angles of incidence of field lines and large wetted areas to distribute power loads uniformly. Additionally, some degree of configurational flexibility is required, so these loads don't vary as a result of changes in the core plasma configuration such as rotational transform, shear, beta, etc. In this study we make extensive use of a code originally developed for the design of the divertor of the W7-X stellarator, Magnetic Field Solver for Finite Beta Equilibria (MFBE), which is a new magnetic topology code developed by E. Strumberger [4], for magnetic configurations which have finite plasma pressure. Prior calculations for W7-X used vacuum magnetic fields outside LCMS. As in those calculations, vacuum magnetic fields are calculated exactly from given coil currents by the Biot-Savart law. In addition to these vacuum fields, MFBE calculates all magnetic fields of finite-beta free boundary equilibria with plasma currents on a grid whose nodes may be arbitrarily close to the plasma boundary. Unlike other stellarators, QAS configurations have a bootstrap current comparable to a tokamak with the same iota, with NCSX having an external transform fraction ranging from 60-81%. This version of MFBE is modified from the version used previously [4], by treating equilibria with toroidal current via the virtual casing principle of Shafranov-Zakharov [5].

For these scrape-off layer studies, the VMEC2000 code described in Section 4.1 is used to determine free boundary finite beta NCSX equilibria. The VMEC2000 code is an energy minimizing equilibrium code which assumes nested flux surfaces and therefore cannot be used to study islands and stochastic regions inside the LCMS. The PIES code described in Section 4.3 and HINT free boundary codes are able to treat islands and stochastic regions, but do not provide this information outside the LCMS. Coupling of the VMEC2000 and MFBE codes allows the LCMS to be found by an iteration procedure involving the toroidal flux parameter, PHIEDGE. The MFBE code obtains as input the Fourier coefficients of potential (at the boundary), flux surfaces and magnetic field from the free boundary VMEC2000. To obtain high numerical accuracy in the calculation of magnetic fields near the LCMS, the number of integration points is adaptive in the distance from the plasma boundary. Some of the interior region near the LCMS is then treated by MFBE to be consistent with external coil currents, and results which disagree with the VMEC LCMS even after iteration on PHIEDGE may be obtained, a numerical error possibly indicative of island formation just within the LCMS, a result which is further supported by the island healing results below.

Here we present calculations of the scrape-off layer field line structure (Figure11-1) for the 1017a2 modular coil design, also designated in Chapter 2 and elsewhere as M3 and which is displayed in Figure 2-4, utilizing the free-boundary VMEC reconstruction of the plasma. The 1017a2 coil set does not have island healing, and is known to have a major island chain within the LCMS from PIES calculations discussed in Chapter 4, see Figure 4-7 The modifications of the coil set to eliminate these islands, as shown by the PIES code calculation such as that illustrated in Figure 4-8 and 4-9 is accomplished by S.Hudson in the 1017c2 modular coil set. The MFBE calculation for the free boundary equilibria obtained with this island healed coil set is presented in Figure 11-2 for comparison. In both cases the VMEC2000 code with input given by li383m3.3k0.0 full current, full beta, but not optimized free boundary solution is used for "as received coils", with the resolution set at NTHETA=16, NZETA=16, MPOL=9, NTOR=5 Here a total of 30 field lines, starting at the bean shaped cross-section midplane at 2mm increments from the VMEC LCMS, are examined. Added to these plots is an approximate conformal vacuum vessel, constructed from the VMEC LCMS, but displaced 10 cm outward, which is used to calculate connection lengths.

Figure 11-1 shows two of a series of Poincaré puncture plots at the toroidal plane at zero degrees and at 60 degrees, with the starting points on the midplane. Field lines and corresponding puncture points are numbered 1 to 30 on the figure going radially outward in starting point. Each line has a color as well as a number, corresponding to the starting point. The VMEC LCMS is represented by the black solid line, the VMEC magnetic axis by the star near the center of each plot, and the conformal vessel is represented by the solid green curve. The routine plot prints out the line number of selected lines at a coordinate determined by location of the puncture point. Thus if the lines were truly ergodized, the line point number would appear randomized, that is the relative location of the starting point would not matter in determining the final position of the line. The lines are followed through 200 toroidal revolutions or until they leave the computational box (which is larger than the plot box shown here). Normally all that would be seen on a puncture plot is the accumulated punctures on the plane from all the calculated toroidal turns. But, here the puncture points which occur during the first toroidal transit of the 3 period machine are tagged with a square symbol, with the labels first, second and third intersection indicative of the period at which the puncture occurs.

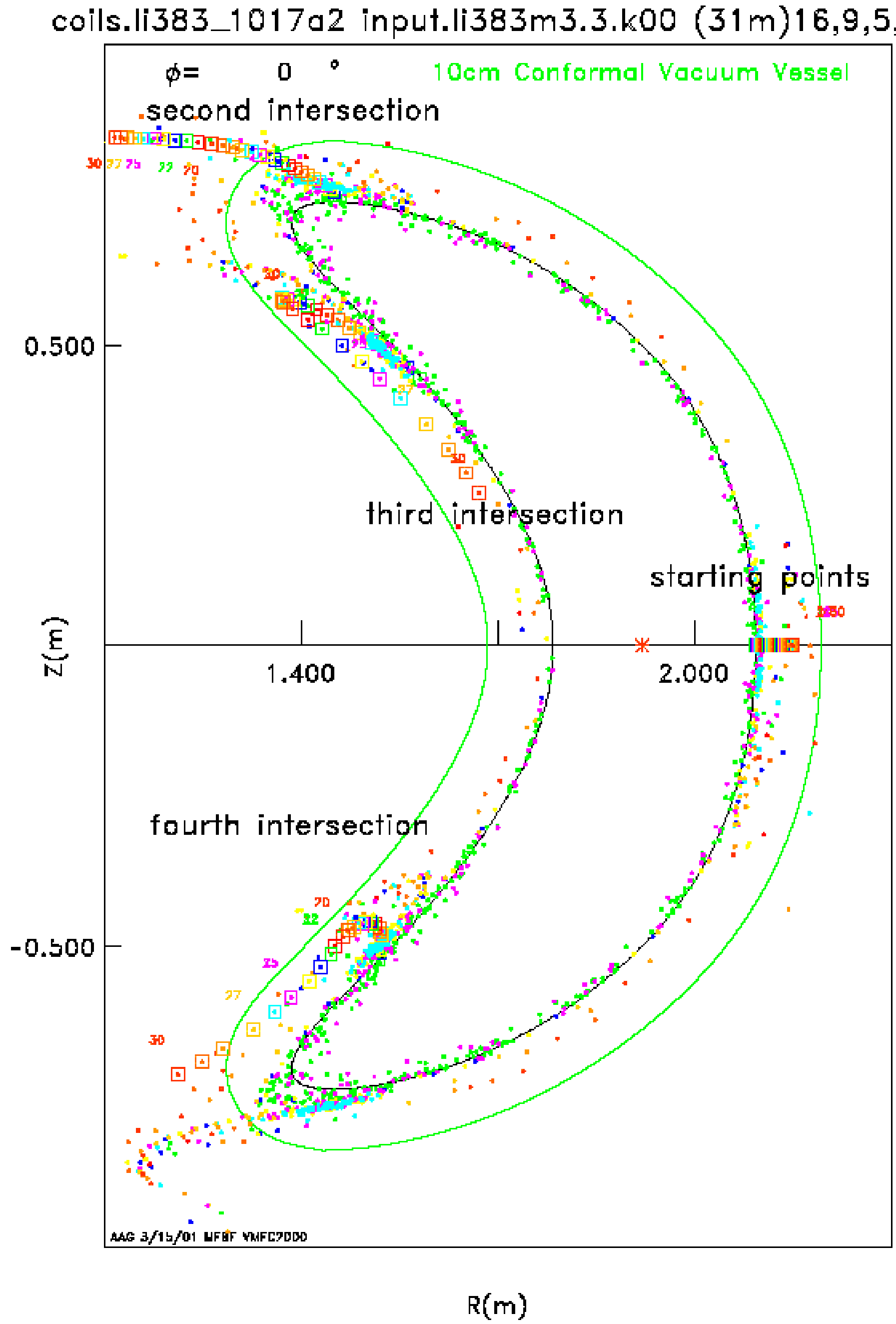

Figure 11-1a. Poincaré puncture plot for the 1017a2 coils without island healing of 30 field lines started at the midplane at a toroidal angle of ϕ = 0 and moving out in increments of 2 mm, followed for 200 toroidal revolutions or until they leave the computational box. The solid black line is the VMEC plasma surface and the solid green contour is the conformal vacuum vessel surface at a distance of 10 cm from the plasma Punctures occuring during the first toroidal pass are highlighted by squares, and labeled by the period at which the intersection occurs

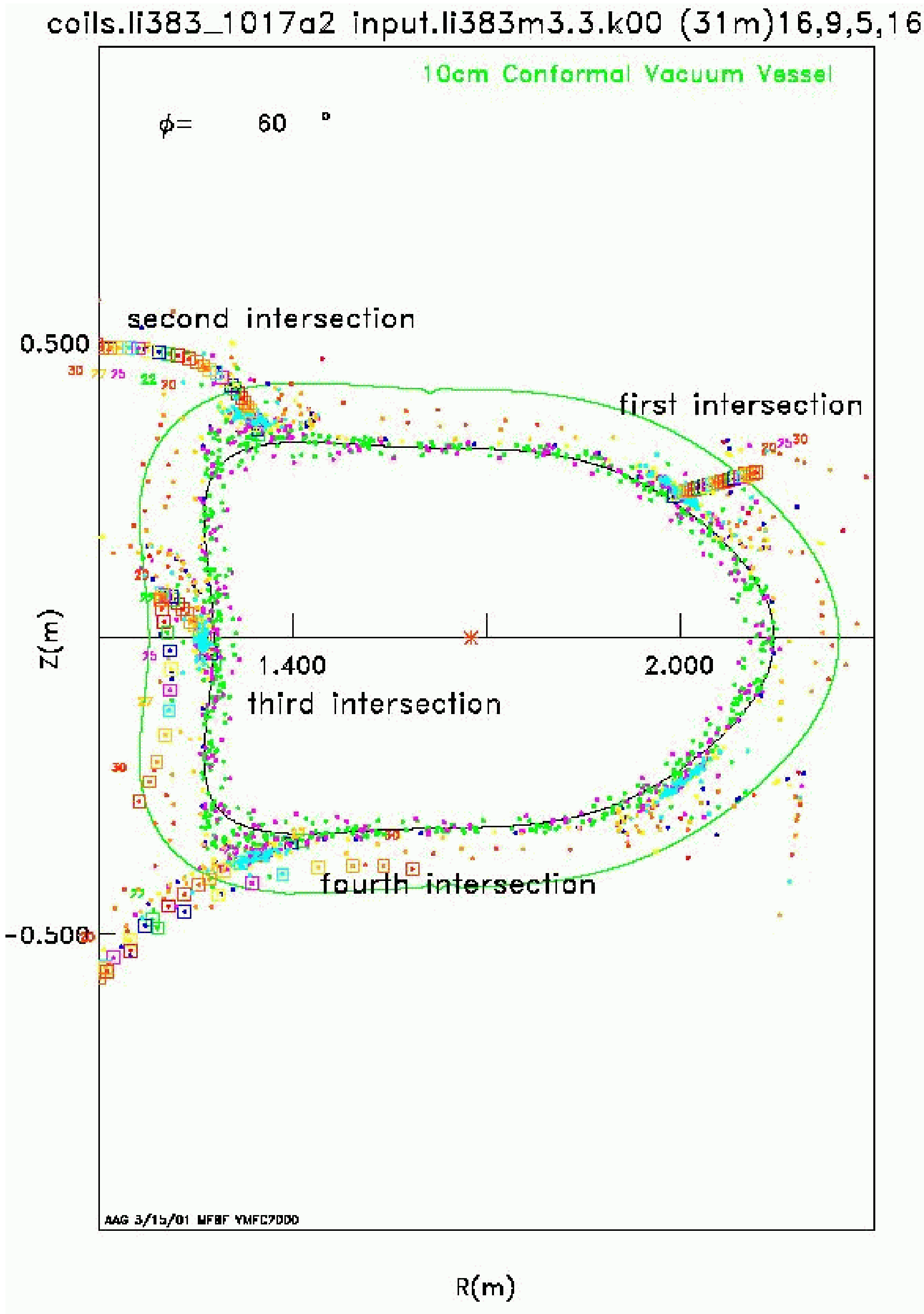

Figure 11-1b. Poincaré puncture plot at the plane located at toroidal angle ϕ =60° , with starting points shown on the midplane of Figure 11-1a, for the same 1017a2 coils without island healing

The order of the field lines continues to be preserved, at least for a single toroidal turn. The maximum excursion (and maximum flux expansion of about 5, obtained by taking the ratio of the line separation at the subsequent intersection to the separation of the starting points) of these lines occurs as the banana-shaped cross-section is approached toroidally, but is at 100 degrees rather than closer to the start of the next period (120 degrees). This maximum excursion is due to the extreme shaping needed to obtain the banana shaped cross-section, and is not a distortion of surfaces due to island structure outside the LCMS. These results do suggest there is a natural ordered-layer structure of the field lines in the edge region, and that these field lines in the edge can thus serve as the coordinate lines and provide connection lengths for plasma edge modeling of a limiter/divertor configuration. With sufficient modification of the wall to accommodate the excursion of these field lines, the diversion properties of the lines may allow a divertor concept based on this flux expansion to be developed for this compact system. Without such a modification, these plots indicate that many of the field lines will have intersected the wall in less than a full period toroidal transit, implying a relatively short connection length from the starting point to the vacuum vessel.

It is seen that there are two ergodic regions, an inner ergodic area characterized by very long connection lengths and radially clustering punctures, for starting points that are within 2 cm of the LCMS, with the closest of these actually having stayed within this region for the full 200 turns toroidally and an outer ergodic region characterized by very short connection lengths (less than a period) prevalent for field lines started beyond 2cm radially from the LCMS. These lines exhibit an ordered layer structure similar to the axisymmetric tokamak up to the first intersection with the wall. Interception by the wall does not stop the field line calculation, and they are seen to return to the region inside the vacuum vessel.

These results were obtained with some island structures observed within the LCMS. Removal of these islands, accomplished by modifying the coils as described in section 2.6, has the effect of altering the ergodicity observed in these calculations in the vicinity of the LCMS. This is illustrated in Figure 11-2 where the island healing coils set 1017c2 replaces the unhealed coils 1017a2 used to calculate Figure 11-1. The VMEC LCMS is then more accurately reproduced by the MFBE field line tracing, and the barely discernable clusters (light blue) of Poincare points outside of the LCMS of Figure 11-1 resolve into a complete chain of 5 islands (orange-red) which are shown enlarged in Figure 11-2c. The islands fit within the confines of a 10cm conformal vacuum vessel and may allow an alternative divertor concept based on island structure.

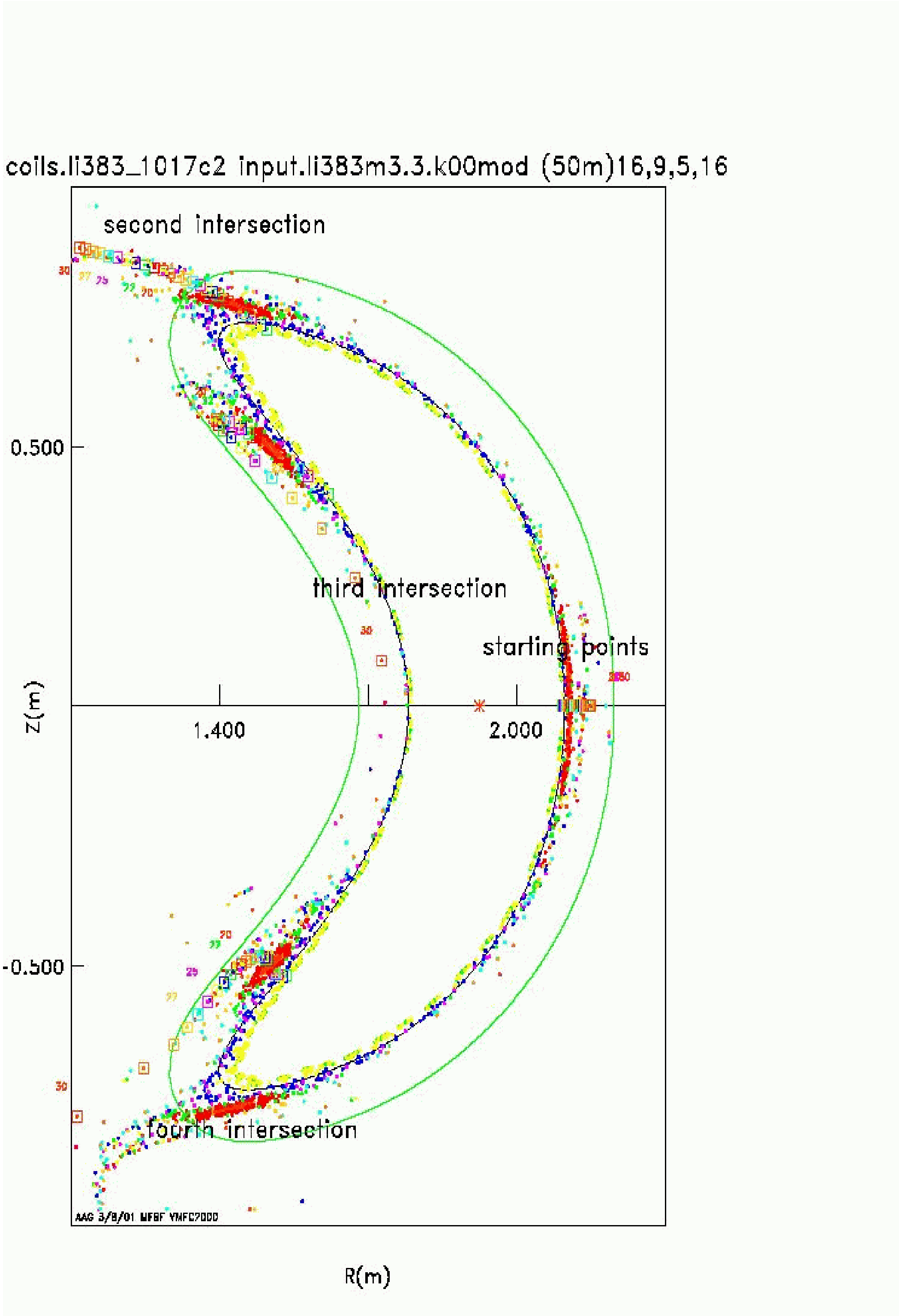

Figure 11-2a. Poincare plots with island healing implemented inside the LCMS (coils 1017c2), for the 30 field lines started at the same locations as Figure 11-1a shown for the plane at toroidal angle of $\phi = 0$ with starting points that move out from the LCMS at the midplane in increments of 2 mm. The ergodicity in the vicinity of the LCMS has now been reduced relative to Figure 11-1, and a distinct island chain is now resolvable

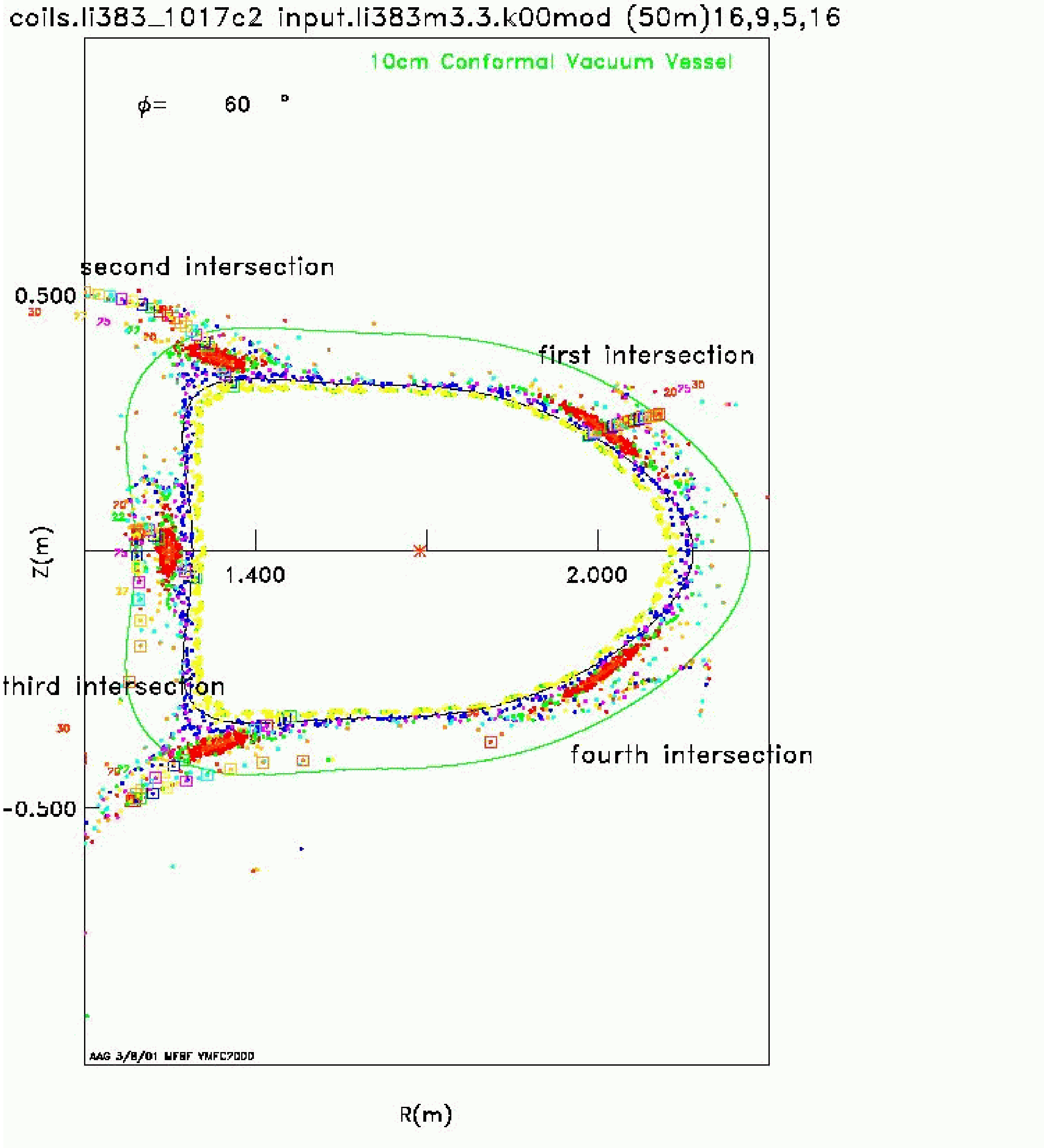

Figure 11-2b. Poincare plots with island healing implemented inside the LCMS (1017c2 coils), for the field lines started at the same locations as Figure 11-1a, with punctures shown for the plane at toroidal angle $\phi = 60°$

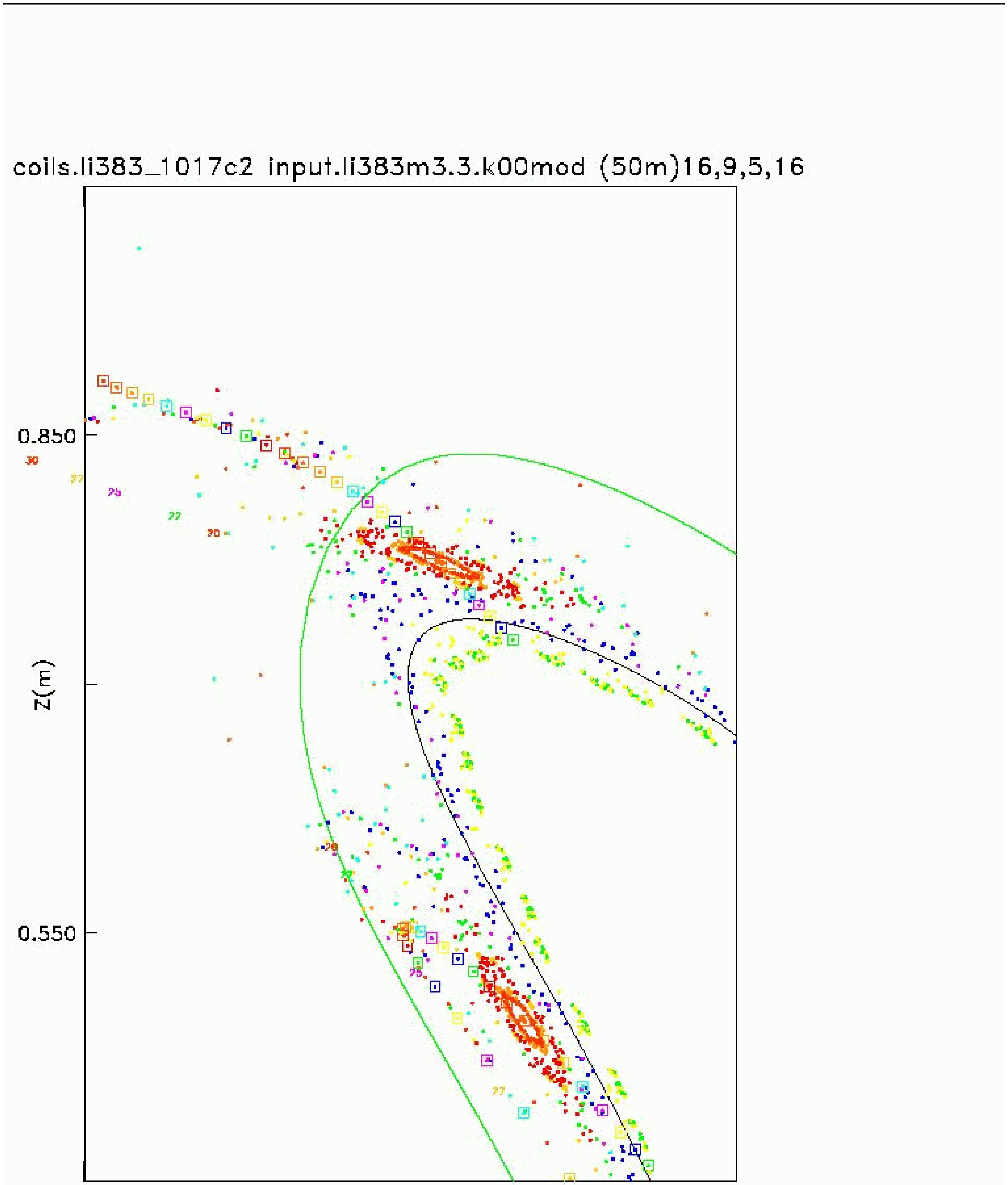

Figure 11-2c. Enlargement of Figure 11-2a region near the banana tip showing island structure between LCMS and conformal 10cm vacuum vessel wall. The squares highlight points from the Poincare puncture at the start of the second period and third period (with starting points at the midplane of the first period). The field line numbers at these highlighted points indicate the preservation of field line ordering, i.e. the field lines are still dependent on the relative position of their starting points at these early punctures, and haven't become ergodic yet. The natural island structure outside the LCMS is now clearly resolved

11.3 Fast Particles Leaving the Confined Plasma Boundary

For the initial operation NCSX will be designed for up to 6 MW of beam power in the 40 to 50 keV energy range. These beams will be injected tangentially in both the co- and counter-directions. As has been discussed above, *(Section 7.32)* the non-zero departure from perfect symmetry in stellarators will lead to enhanced levels of beam ion losses above those present in an equivalent axi-symmetric tokamak. The loss patterns of beam ions on the vacuum chamber wall might require wall armor to handle the respective heat fluxes and to minimize the generation of impurities. Within the Monte Carlo slowing-down model described in Section 7, the exit locations, exit times, pitch angles and energies of the beam ions, leaving the outermost closed flux surface, are recorded. Assuming that beam ions then move rapidly through the open outer flux region, the recorded parameters are used in estimating power loading patterns on the vacuum chamber walls.

As discussed above, some of the characteristics of a slowing-down beam for the parameters $n(0) = 6 \times 10^{19}$ m^{-3}, $T_e(0) = T_i(0) = 2.4$ keV have been calculated *(see Section 7.32)*. As an example, Figure 11-3 shows a histogram of the energy distribution of the escaping beam ions injected with 40 keV energy.

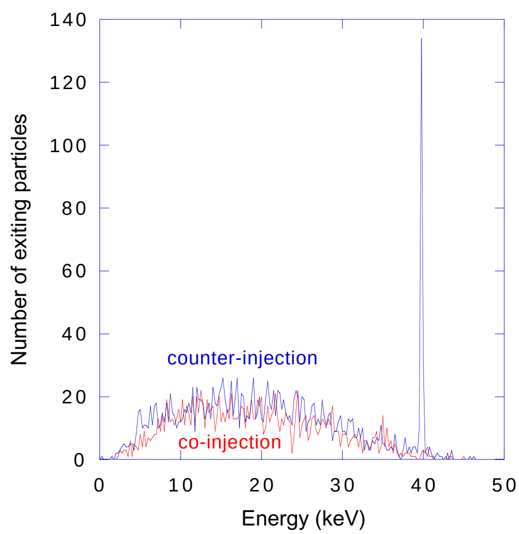

Figure 11-3. Energy spectrum of beam particles exiting the last closed magnetic surface

As can be seen, the energy losses are characterized by a broad distribution centered around 15 - 20 keV for both co- and counter- injection. The counter-injected ions also show a very sharp peak at the injection energy, presumably associated with prompt losses. It is important to know how much of the total injected energy is lost in fast particles, which is dependent on the injection energy. The result presented in Figure 11-3 has been based on 40 keV ion energy. The beams anticipated for NCSX will be capable of going up to 50 keV, but will also include lower energy components. In Figure 11-4 we investigate the variation of beam losses with injection energy as described above *(Section 7.32)*.

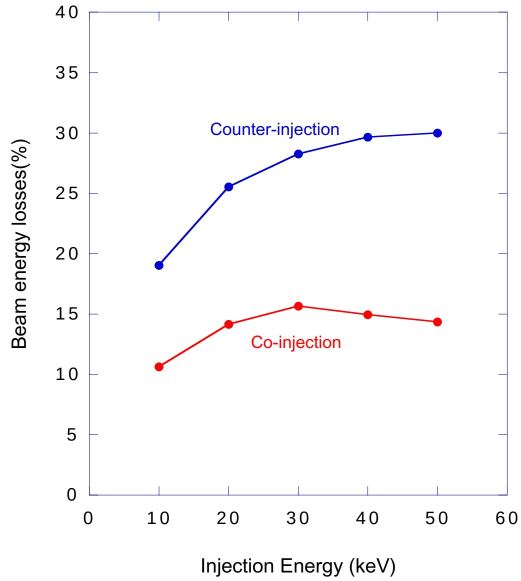

Figure 11-4. Variation of beam energy losses with injection energy for a machine design point at R_0 = 1.4 m, <B> = 1.23 T, n(0) = 8.5 x 10^{19} m^{-3}, $T_e(0) = T_i(0)$ = 1.58 keV

Based upon the current model, exit locations and energies are shown in Figure 11-5 for a typical case. Here the exit locations are plotted in Boozer poloidal and toroidal angle coordinates for the outermost flux surface. Colors are used to indicate the energy at which the fast ions leave the surface. As can be seen, most of the ions leave at intermediate energies from 10-20 keV, in similarity with Figure 11-3.

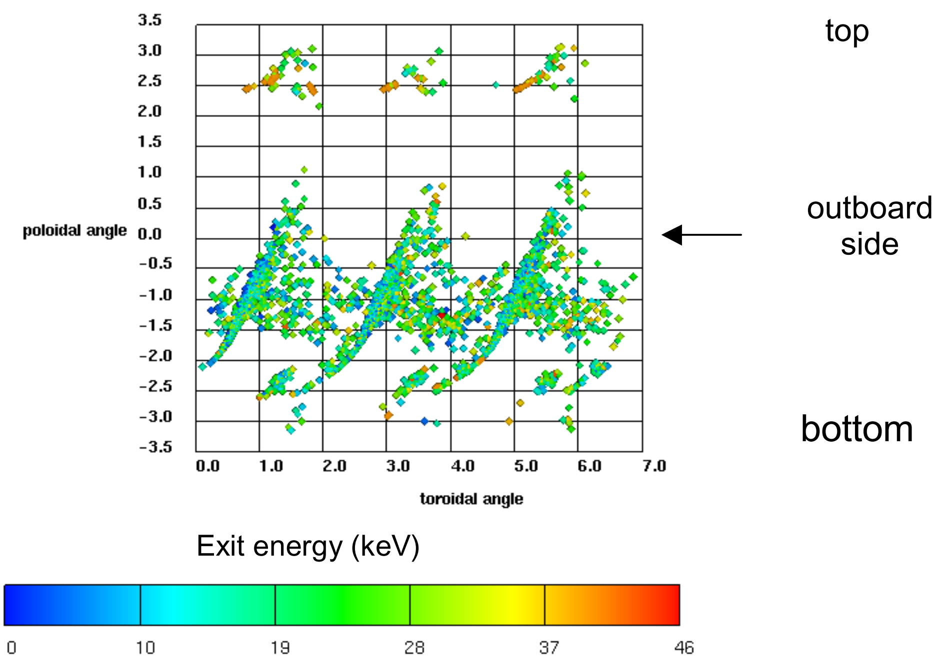

Figure 11-5. Location and energy spectrum of beam losses on outer surface in 2D Boozer coordinates

The fast ion losses are primarily concentrated in helical stripes on the bottom of the vacuum vessel with one stripe per field period (shifting to the top with reversal of the magnetic field

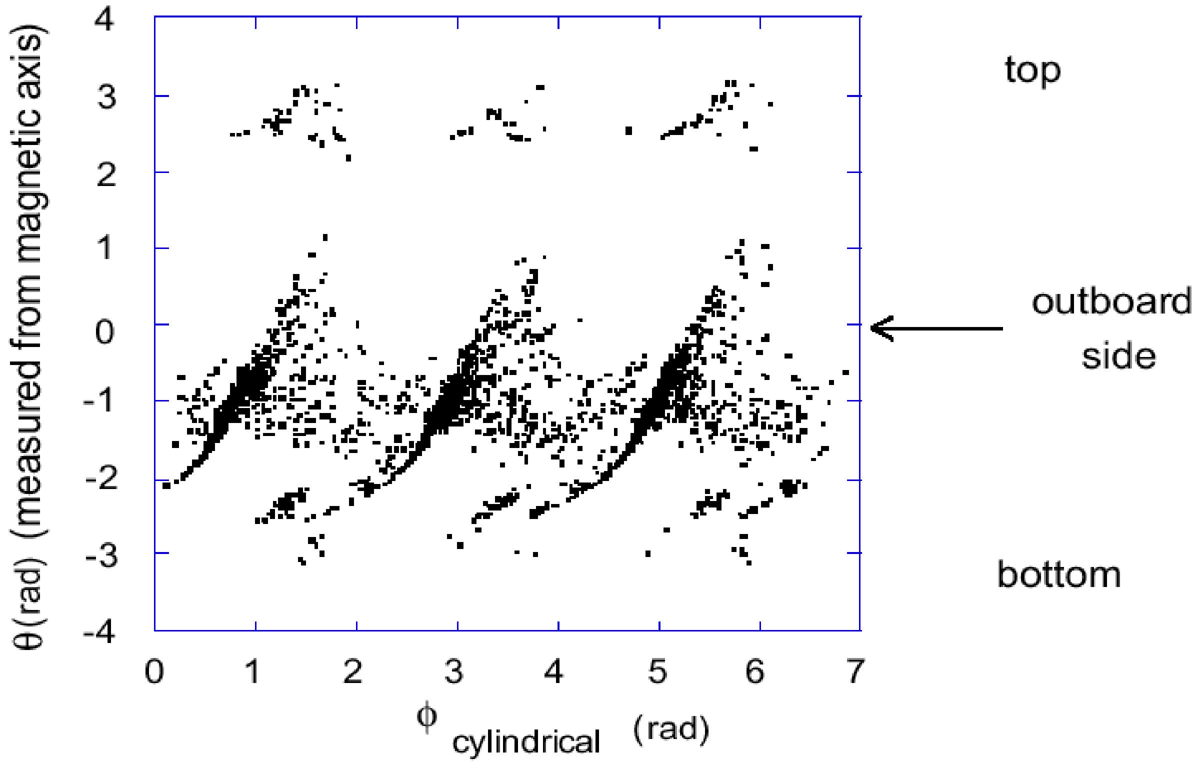

Figure 11-6. Location of beam losses on outer surface in 2D real space coordinates

direction). We have also transformed this data into real-space coordinates. In Figure 11-6 we plot the data of Figure 11-5 vs. the normal cylindrical azimuthal coordinate, $\phi_{cylindrical}$ and a poloidal angle θ, which is equal to $\tan^{-1}[z/(R-R_0)]$.

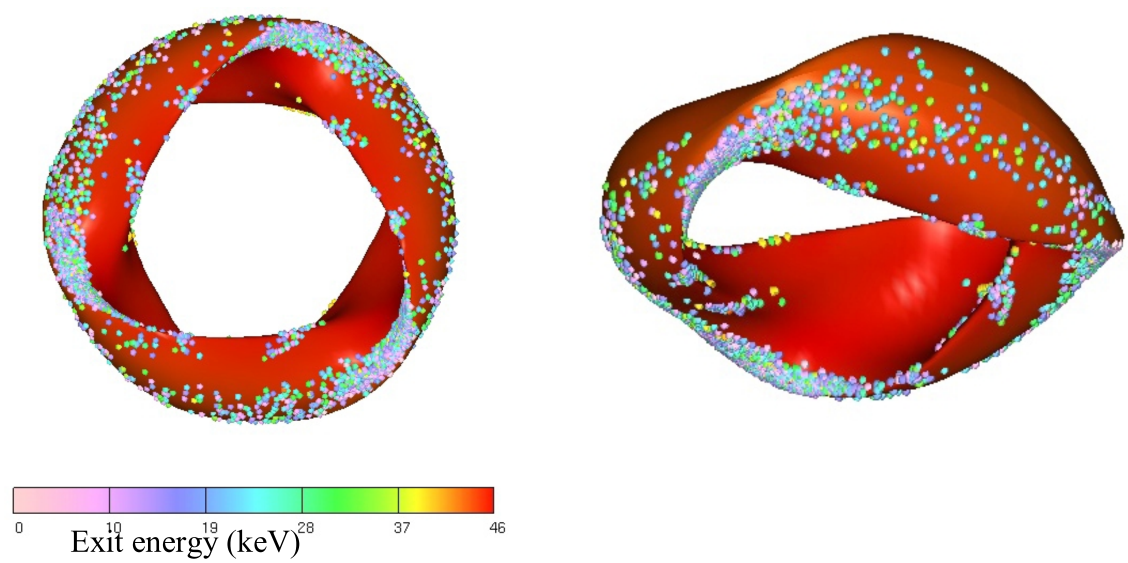

Figure 11-7. Location and energy distribution of beam losses on outer surface in 3D

Finally, we have plotted the ion loss locations on the three-dimensional outermost flux surface (Figure 11-7) as obtained from the VMEC stellarator equilibrium code. The flux surface is shown in red and the ion exit locations are color-coded according to the ion's energy at the time it passes through the flux surface. Again, it can be seen that the losses are somewhat concentrated, motivating the design of protective structures at these locations.

11.4 Heat Flux Estimates Including Cross-Field Diffusion

The initial design point for the NCSX scrape-off-layer (SOL) plasma assumes attached conditions from the last-closed-magnetic-surface (LCMS) to the material targets. This can be achieved with sufficient field-line length between the LCMS surface and the targets, $L_c > 100$ m, referred to as the connection length. Under these circumstances the SOL plasma will be at moderate to high temperature, *e.g.* , 100 - 200 eV at the LCMS and 20 - 50 eV near the targets (see below). Energy transport in a SOL at these temperatures will be dominated by electron conduction parallel to the magnetic field lines. Therefore, initial estimates of the heat flux profile on the targets can be obtained by following a sufficient number of field lines from the region of the LCMS where the power enters the SOL to where the field line strikes a surface. The density of field line strike points gives the estimate of the heat flux profile (see Section 11.2).

A heat flux estimate obtained solely from field line tracing overestimates the peak to average heat flux ratio and underestimates the radial and toroidal extent of the required high heat flux target surfaces on the wall because it ignores cross field transport in the SOL. For sufficient field line length and SOL turbulence the cross field transport can broaden the heat flux profile which finally reaches the target surface. The broadening can be both in the toroidal and the poloidal directions so this effect can have a significant impact on the required design of high heat-flux target-components. The effect of broadening of the profile compared to what would be calculated from unperturbed field line tracing has been observed experimentally on the W7-AS stellarator [7]. Of course, this broadening is enhanced by the stochastic magnetic-field layers and the magnetic island X-point structures in the SOL that are typically produced in W7-AS. However, even in the relatively ordered NCSX SOL fields, the field lines beginning close to the LCMS have sufficient connection length that some broadening of the heat flux profile is expected.

The technique used by the NCSX edgegroup to estimate the effect of cross field transport broadening of the heat flux is to couple a field line tracing algorithm with a model for "diffusion" of the field lines. The computation is set up to follow unperturbed field lines for a specified parallel distance and then displace the radial position of the field line before continuing the parallel field line tracing. The displacement distance is calculated to simulate an expected energy transport coefficient in the SOL. The displacement direction is taken from a random polar distribution in the plane perpendicular to the field line direction.

The field line tracing with diffusion technique produces substantial broadening of the strike point distribution in calculations for the W7-X stellarator design [6,7] . The setup for this example begins with the assumption that the cross-field scale width of power in the SOL is $\lambda_\perp$ =

1.5 cm. Then assuming a balance between parallel and perpendicular diffusive transport in the 2D energy balance equation, one derives that $\chi_{||} / \chi_{\perp} \sim (\lambda_{||} / \lambda_{\perp})^2$. If one assumes the parallel scale-length for power in the SOL is approximately $L_c /4$, then for an average connection length of approximately 100 m in W7-X, one obtains $\chi_{||} / \chi_{\perp} \sim 3 \times 10^6$ as in the example of Reference 7. The code simulations for this example used 0.001 m displacements of the field lines after each 0.3 m field-line length. This implies over 300 displacements along a field line of average connection length, and 0.3 m radial displacement of the field line if all the displacements were in one direction. Even with random displacement direction it is not surprising that substantial spreading of the profile of strike points on the wall was calculated.

The computational algorithms that perform this calculation for the W7-AS and W7-X stellarator designs will be adapted to calculate the heat flux broadening for NCSX. The average field line length will be obtained from the unperturbed field line tracing results of Section 11.2. Since NCSX is a toroidal device with a combination of the properties of tokamaks and classical high aspect ratio stellarators, our knowledge of the anticipated perpendicular scale widths for power and particle flux in the SOL is quite limited. As a result we will need to do multiple simulations of field line tracing with the diffusion model for a range of perpendicular transport coefficients to scope out the requirements on the high heat flux target designs. The speed of the field-line tracing and diffusion model calculations will be increased by converting them to parallel computers so that it will be possible to trace an adequate number of lines (~1000) for a sufficient number of transport coefficient cases to guide the design requirements of the targets.

11.5 First Wall Configuration and Materials

The configuration of the first wall is to a limited degree conformal to the plasma. The reason for the vacuum vessel being only of limited conformal shape is for operational flexibility and due to the numerous ports, necessary mainly for beam injection and diagnostics, generate large deviations from conformity. This can be seen in Figure 11-8 which shows cross sections of the vacuum vessel and the plasma at $\phi = 60°$ (bullet-shaped) and $\phi = 0°$ (bean-shaped). This figure shows a typical example of how little of the bean-shaped plasma cross-section is actually surrounded by a conformal wall surface, while the situation is obviously different for the bullet-shaped cross-section. Figure 11-9 provides a plan view of the plasma and vacuum vessel that also demonstrates the large deviation of the vacuum vessel from the conformal shape.

The main material of the vacuum vessel is stainless steel and the plasma-facing components will be made of graphite or carbon-fiber composite (CFC) material. The ideal case would be to cover the whole first wall with CFCs; this would take care of neutral beam shine-through, energetic particle losses, and limiter/divertor baffles all together. But, this ideal case would be fairly expensive and also not needed for the first phase of machine operation with an input power of 3 MW for <0.30s.

To stay within the budget for the initial machine configuration, the plan is to start by covering selective areas: for neutral beam armor, inboard limiters centered at $\phi = 60°$, and neutral particle baffles centered at the $\phi = 0°$ cross-sections.

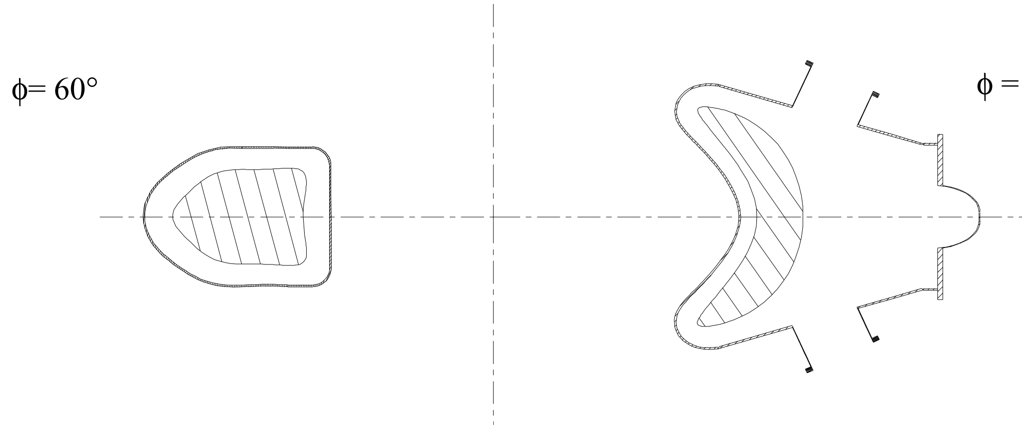

Figure 11-8. Plasma and vacuum vessel cross-section at the ϕ = 0° and ϕ = 60° cross-sections

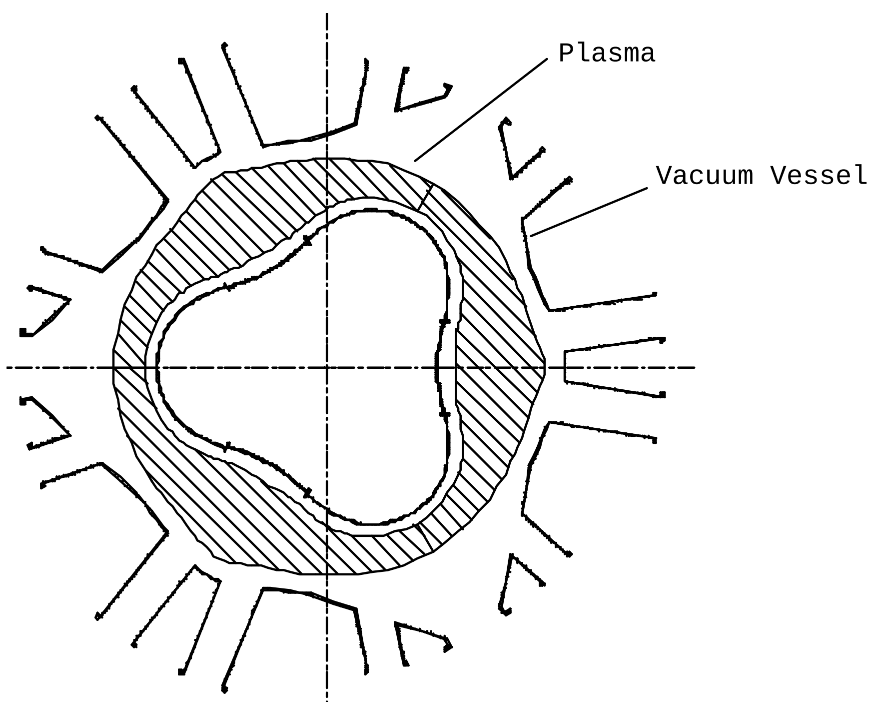

Figure 11-9. Plan view of the plasma and the vacuum vessel. It shows clearly the large deviation of the vacuum vessel from the conformal shape

11.6 Initial Power Handling System

There are several requirements that impact the NCSX limiter/divertor configuration. The power-handling requirement (i.e. power and pulse length) will be a factor in selecting the heat removal surface area. The heat load requirement for initial operation is 3 MW for a pulse length of ~0.30 sec. Data from past experiments shows that a peak heat load up to about 30 MW/m^2 can be absorbed by graphite composites. If we assume a peaking factor of three, we will require about 0.3 m^2 of heat removal area.

The need for symmetry will impact the toroidal and poloidal location of the limiters and divertors. This requirement translates to one heat removal surface per period with vertical symmetry and an area of at least 0.1 m^2 per period. In addition, the need to limit the neutral penetration to the plasma core will restrict the location of the neutral sources to broader plasma cross sections. The limiter locations will need to take into account the possible location of an RF antenna at the small major radius side of the bullet cross section.

The neutral beam injection configuration will require a system of beam armor at the locations where the beams impinge on the wall. In addition, the injection process will result in a fast ion loss as discussed in Section 11.3. The wall will need to be protected at the locations of high ion loss trajectories. The ion orbit studies indicate relatively broad regions of ion impingement on the wall.

In general, a range of options can be accommodated by the mechanical configurations being considered for NCSX. As the project progresses into more detailed design phases the local mechanical requirements for the limiters and divertor will need to be factored into the design process. We have selected a preferred limiter/divertor configuration for initial operation to demonstrate feasibility and support the costing exercise. In addition, this preferred configuration could be used to demonstrate the compatibility of the plasma facing components with the overall configuration and with physics objectives.

The preferred initial limiter/divertor configuration integrates the limiter, divertor and wall armor into one heat removal configuration. The specific approach will be to mold a range of shapes from a graphite weave to cover the required locations. We expect that the required coverage is about 50% of the first wall area. This approach can be used to mimic localized-fixed limiters by molding a shape that protrudes from the surrounding wall covering. The attraction of this option is that it can cover a multitude of heat removal and wall protection needs while minimizing performance uncertainties.

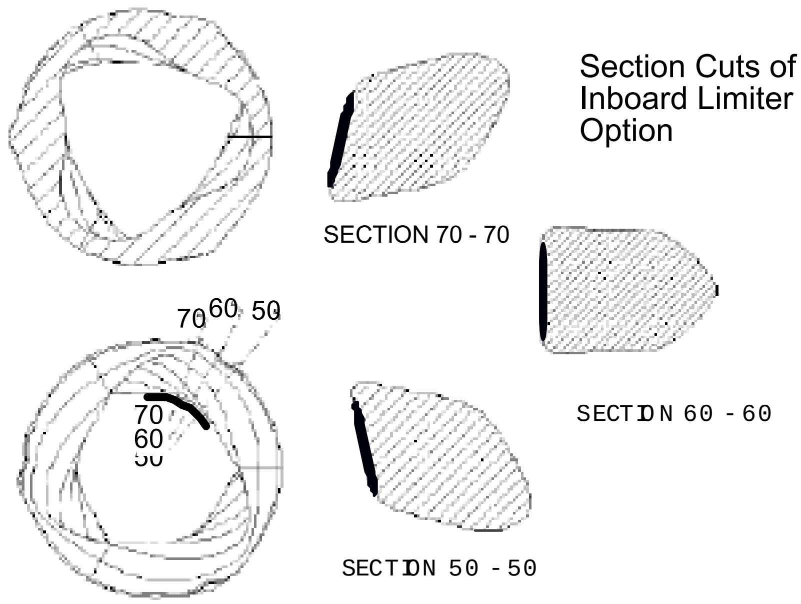

Figure 11-10. Inboard limiters 'centered' around the ϕ = 60° cross-section (one per field period)

The region selected for locating limiters is the small major radius side of the three bullet cross sections, as shown in Figure 11-10. The contact area will have the shape of a long rectangle oriented at a shallow angle to the horizontal so as contact a relatively flat surface. One attraction of this location is the existence of this flat region. A second attraction is that this location will provide reasonable neutral shielding for the plasma core. A third attraction is that this location should have reasonable magnetic shape stability. As stated above it is possible that an RF antenna will be located in this region in one magnetic period. If this is the case we will integrate the antenna power and particle protection in this period with the limiter function.

In addition to the limiters just described, we propose to locate a heat removal surface at the tips of each bean cross section (i.e. six locations). This configuration should function as a divertor. The location of heat removal surfaces near the bean tips will take advantage of the expanded flux in this region to reduce the local heat flux. An assessment is being made of whether heat removal surfaces in this location can be movable to increase flexibility. Experiments with this configuration should provide a data base to support the design of a future divertor upgrade with the potential for neutral pumping.

A research program to develop a data base for plasma facing components in this stellerator configuration will play an important role during the initial physics operations phase. This data will contribute to the design of upgrades in the plasma facing component to support higher power operation. Of particular importance will be the development of an understanding of the region outside the last closed flux surface and the geometric requirements for divertor operation.

As stated above, the location of heat removal surfaces near the bean tips will take advantage of the expanded flux in this region and provide valuable experience for future upgraded divertor implementation. An assessment is being made of whether heat removal surfaces in this location can be movable to increase flexibility. The location of a fixed limiter at the midplane of the bullet section will provide good neutral shielding behavior at a location with relatively smooth surfaces. Future studies will determine the physics flexibility to accommodate a range of plasma motion relative to the fixed limiter location. To the extent that we can move the plasma relative to the limiter without significantly degrading the physics performance we can experience the advantages of a movable limiter along with the advantages of a location at small major radius.

11.7 Divertor Upgrades

Important future improvements of the divertor/limiter system will include upgrades of the power handling capability and divertor baffling and pumping.

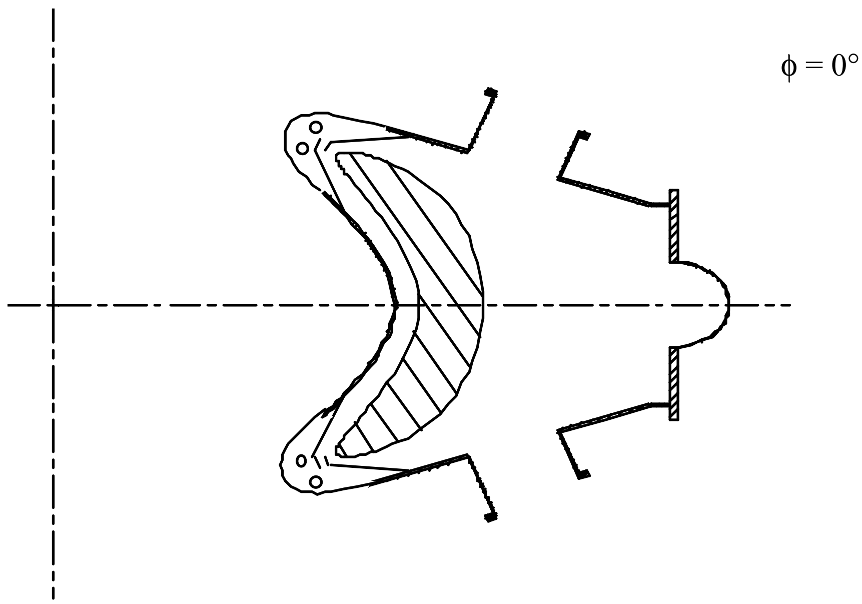

Figure 11-11. Divertor upgrade including neutrals baffles and pumping

The divertor baffles have to serve two purposes. They represent the main divertor plates, i.e. they are designed to handle about 80% of the thermal power leaving the main plasma by convection and conduction. At the same time they are designed to confine neutrals mechanically and either direct them back into the boundary plasma or guide a certain fraction behind the baffles into the divertor pumping plenum. Figure 11-11 shows a schematic view of this arrangement. Pumping could consist of titanium gettering or cryo-pumping. Note: the baffles and pumps are not toroidally continuous, but extend only over a certain toroidal length 'centered' around $\phi = 0°$.The actual divertor baffle and pumping system will be designed in the future, guided by neutrals and plasma transport codes (DEGAS2, etc.).

11.8 Neutral Transport Calculations

Fully three-dimensional simulations of neutral particle behavior in NCSX will be needed in its latter design stages and as part of experimental analysis during machine operation. Although three-dimensional Monte Carlo neutral transport codes exist (e.g., DEGAS 2, EIRENE), no tools exist for easily converting external descriptions of the stellarator geometry and plasma into the data structures used inside those codes. The existence of a large effort at IPP-Greifswald to develop a three-dimensional fluid plasma code (BoRiS) provides a clear path forward for not only establishing the needed interface for the neutral transport codes, but also for setting up a coupling between them and the BoRiS code.

The near-term need (e.g., for this report) is for rough estimates of neutral penetration lengths. Tokamak experience suggests that having a significant fraction of the recycling neutral atoms and molecules reaching surfaces well inside the last-closed magnetic surface leads to unacceptably low core energy confinement times. Since the bulk of the recycled neutrals leave the surface with a cosine distribution (i.e., peaked about the normal to the material surface), the greatest penetration will be achieved in the same poloidal plane as the recycling surface. Consequently, toroidally axisymmetric neutral transport calculations can place an upper bound on the neutral penetration distance.

The DEGAS 2 Monte Carlo neutral transport code [8] is used here to perform such calculations, first with recycling at an outboard limiter and then with the recycling occurring at a divertor baffle. The setup codes used to generate the DEGAS 2 input files permit considerable, but not complete flexibility. Hence, the correspondence between the limiting and baffling structures used in DEGAS 2 and those proposed elsewhere in this document as the actual NCSX plasma facing components is less than perfect.

The plasma shape, specified in terms of a "moments" representation for R and Z, was obtained via a VMEC equilibrium for the li383 case. For the purposes of this document, the calculations use the poloidal cross-section corresponding to a toroidal angle of 0 degrees ("bean" cross section). In general, the angle used can be arbitrarily chosen. For simplicity, a uniform mesh of 30 points in the poloidal angle was assumed.

The VMEC equilibrium provided contained many more flux surfaces than were necessary for the neutral penetration calculations. The set was reduced in a semi-arbitrary manner so that the maximum distance between adjacent surfaces was 5 cm. This procedure resulted in a total of 17 surfaces for the bean cross section.

The vacuum vessel (VV) shape was likewise specified via a moments representation. To increase radial resolution between the last closed magnetic surface (LCMS) and the VV, four additional surfaces were inserted via interpolation in between.

The remaining step in establishing the geometry for neutral transport is the specification of the recycling locations. As this setup code is currently constructed, the minimum size and exact location of these surfaces is controlled by the poloidal angle mesh. One set of calculations described here uses an outboard limiter assumed to consist of two poloidal mesh segments extending from the VV to the LCMS. A second set utilizes a divertor target composed of four poloidal mesh segments centered about the bottom of the bean cross section and located just in front of the VV.

The plasma profiles used in these initial calculations (Figure 11-12) were constructed as described in Section 8.3, using an assessment of the W7-AS experimental database for the edge and scrape-off layer conditions [9].

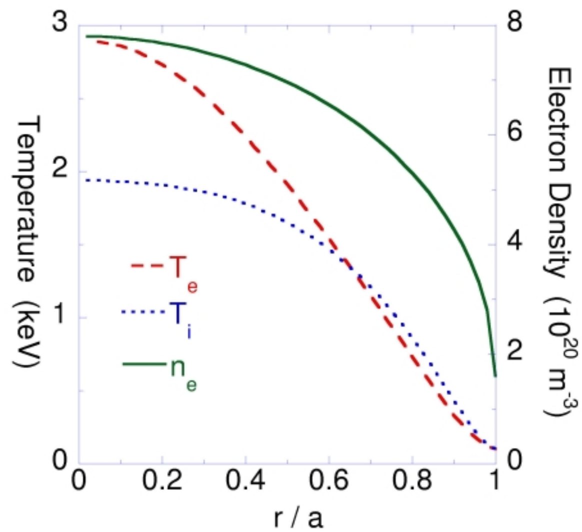

Figure 11-12. Core plasma temperature and density profiles used in the neutral transport calculations were obtained via the neoclassical transport analysis of Section 8.3

These were interpolated onto the core plasma surfaces (these calculations are in a cylindrical geometry; here, r/a is equated with the square root of the ratio of the local to LCMS toroidal flux). A scrape-off length (relative to the LCMS, locally in physical space) of 2.2 cm for both density and temperature was used. The resulting electron density and temperature profiles are shown in Figure 11-13.

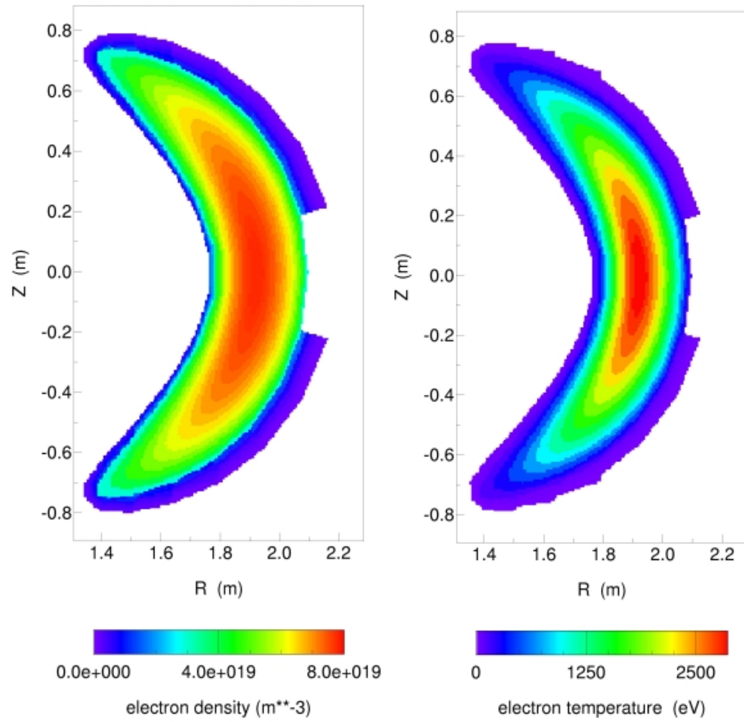

Figure 11-13. Two-dimensional plots of the electron density and temperature data used in the neutral transport calculations. These plots show the outboard limiter as the "missing" white region centered about the midplane

The white area on the right side of the cross section corresponds to the outboard limiter (this region contains plasma in the second simulation with recycling at the divertor baffle).

The atomic physics used includes D_2 dissociation and ionization, D charge exchange and ionization. All of the hardware is currently assumed to be carbon. The only plasma-material interactions used are reflection and desorption (for everything not reflected). A fixed D recycling source (2×10^{21} s^{-1}) is taken to be spread uniformly over the recycling surfaces in these two simulations.

Figure 11-14 shows the D density and D^+ ion source rate for the first simulation featuring recycling at the outboard limiter. Note that the peak neutral density and ionization source occur inside the closed flux surfaces (since the limiter is positioned at the LCMS). The scale lengths for both the density and the ion source rate in front of the limiter are about 0.8 cm. The neutral density at the magnetic axis is roughly 10^{-3} of the peak value; the ion source rate there is 3×10^{-4} of its maximum value.

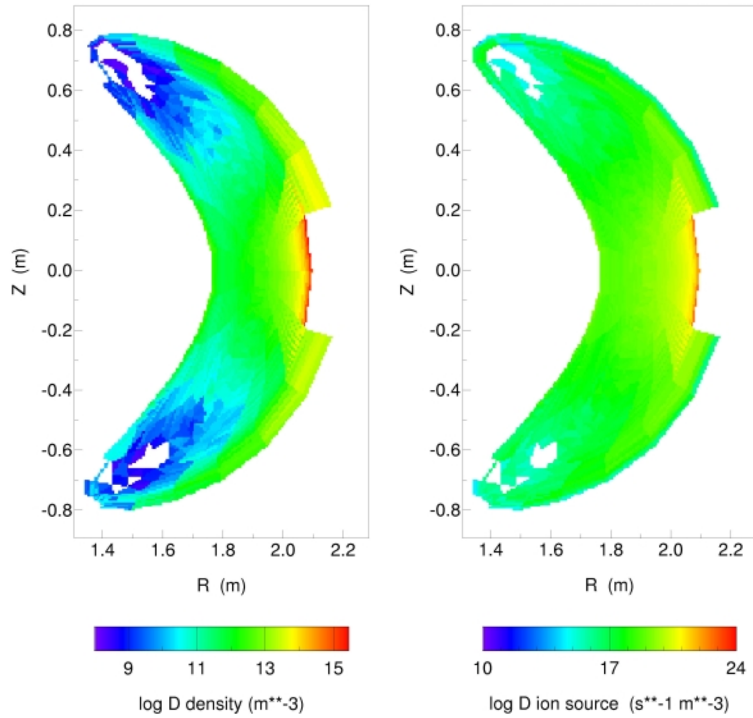

Figure 11-14. Two-dimensional plots of the log of the neutral atom density and the ion source rate obtained with recycling at an outboard limiter. To facilitate computation of the logarithm, factors of 10^9 and 10^{10}, respectively, were first added to the data

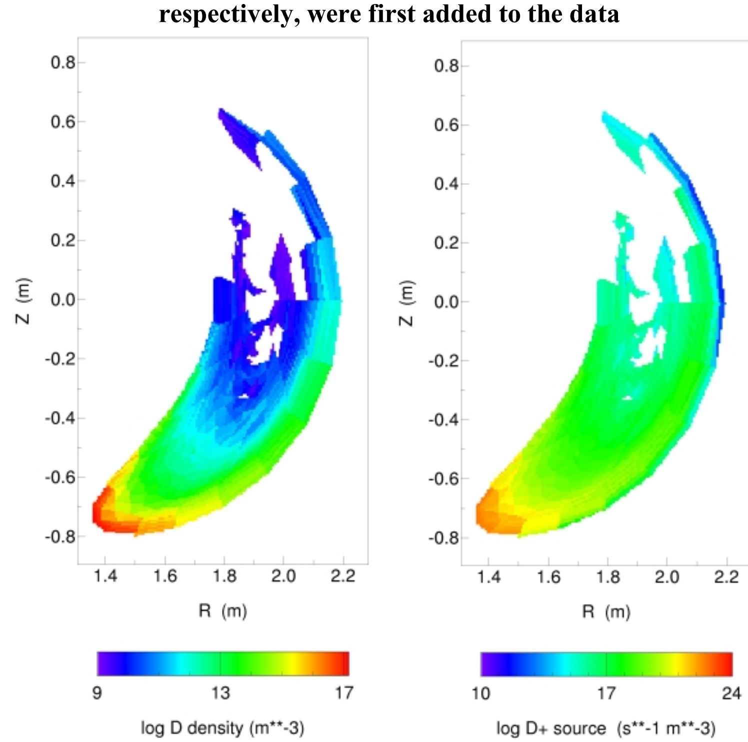

Figure 11-15. Two-dimensional plots of the log of the neutral atom density and the ion source rate obtained with recycling at lower divertor. To facilitate computation of the logarithm, factors of 10^9 and 10^{10}, respectively, were first added to the data

Figure 11-15 shows the D density and D source for the case featuring recycling at a divertor baffling surface positioned at the lower tip of the bean cross section. In this case, the density and ionization source inside the LCMS are much smaller (more than one order of magnitude) than in the limiter case. The maximum neutral density inside the LCMS is a factor of 0.09 times the overall peak value; the maximum ion source rate there is 39% of the overall peak. Both the neutral density and the ion source rate are effectively equal to zero at the magnetic axis. Thus, it is very important to ensure that recycling occurs in the peak region and not the midplane.

11.9 Edge Modeling

11.9.1 Self-Consistent Edge-Plasma Transport Modeling

Estimating high heat-flux locations and magnitudes on the vessel wall via magnetic field-line tracing is described in Section 11.4, including diffusion to model turbulent cross-field thermal transport. While these are important tools to indicate where to place protective tiles on the walls, experience with tokamaks shows that a more complete transport model of the edge plasma, including particle, momentum, and energy flows, is needed to understand the variations that are possible for the heat-flux profiles, and for the particle fueling that is related to the core density limit. The interaction between the plasma and neutrals is the key issue here. Such a model will contribute to decisions about upgrades to the NCSX power and particle handling hardware including the most effective location of baffles to control fueling. A self-consistent model will provide vital information on the type and position of edge-plasma diagnostics, and is also needed to predict the level of impurities that can enter the core.

To obtain the self-consistent description of the edge plasma and neutrals, we are collaborating with the IPP Greifswald group in the development of a 3D stellarator transport code known as BORIS. The Greifswald group, which includes 4-5 people dedicated to this task, has already designed the basic code structure and has obtained some preliminary results based on the electron and ion energy equations [10]. Our role is to provide expertise in the areas of iterative solvers, fluid neutral description, **E**x**B** drifts, and possibly parallelization. At the same time, we will adapt the code to the NCSX geometry and perform self-consistent edge-plasma calculations. We anticipate that initial results will be available for NCSX by the end of fiscal year 2001, but this modeling work and development will evolve for a number of years, finally providing a close contact between theory and experiment.

For the BORIS code, the Braginskii-like magnetized fluid equations are solved for the plasma density, parallel velocity, electron and ion temperatures, and the plasma current. The parallel transport is taken as classical, while the cross-field transport has an important turbulence component as discussed in the next section. The neutrals will initially be described by a set of flux-limited fluid equations. A finite-volume discretization is used, together with an implicit algorithm for the resulting large matrix problem.

Aside from the substantial complication associated with the 3D nature of the problem, the BORIS components are the same as we have developed in the 2D UEDGE transport code. Thus, we should be able to use this experience to great advantage while at the same time leveraging for NCSX the substantial effort being applied to this work at Greifswald. We expect to be able to characterize the edge-plasma in the same detail as we have done for tokamaks where there is generally a good correlation between models and experiments. In addition to edge-plasma characteristics and heat deposition profiles, this work will also provide the edge-plasma for Monte Carlo calculations with DEGAS2; the initial BORIS neutrals model is a fluid description and the Monte Carlo neutrals calculations will be an important refinement. Also, impurity ions will be added to the description in the next year.

We have already begun our collaborative work with the BORIS code through two visits to IPP Greifswald, and a three-week visit to LLNL last spring by two of the BORIS developers. These collaborative visits will continue in order to ensure a close connection with the code developments. This connection is further strengthened by joint work on the BOUT turbulence code described in Section 11.9.2.

A second method based on a Monte Carlo technique has also been used for advancing the plasma transport equations in 3D for stellarators [11]. This meithod is being developed and validated. We will monitor its progress and may collaboratively pursue it at a later time.

11.9.2 Edge-Plasma Turbulence Modeling for the NCSX

A very important component of the edge-plasma characterization is to understand, at a fundamental level, the nature of the turbulence and resulting cross-field transport. Not only does this impact the width of the scrape-off layer plasma, but it can also give rise to an edge transport barrier as in the H-mode transition for tokamaks. At the same time, the turbulence simulations need to begin with full edge-plasma profiles from two-point estimates, transport simulations, or experimental data. For the short term, turbulence simulations can give important information on the toroidal and poloidal distribution of power leaving the LCMS which can be used to improve the wall power-deposition calculations even using the field-line tracing models.

Again, the turbulence work should benefit substantially from a collaboration with IPP Greifswald, but at this time, we have the basic 3D turbulence code that has been used to describe edge-turbulence in tokamaks called BOUT [12], and the Greifswald group wants to help modify it for stellarators. To aid in this work, R. Kleiber from IPP Greifswald will visit LLNL for three months this spring (2001) to adapt BOUT to the stellarator geometry. With a successful completion of this work, extension to NCSX should be straightforward, but the computational work will be extensive.

We plan to use the results of the turbulence modeling to determine the turbulence cross-field diffusion coefficients for use in the transport code and to learn how these scale with parameters and changes to the equilibrium. In the long term (several years), we envisage a more direct coupling between the turbulence and 3D transport simulations. In addition to giving a fundamental characterization of the scrape-off layer plasma, the turbulence calculations should give an understanding of possible core transport barriers in the stellarator edge; this is of major importance to any confinement device.

11.9.3 Implications of Short vs. Long SOL Connection Lengths on Core Confinement

11.9.3.1 Summary

The connection length, L_c, of field lines in the SOL outside the last closed magnetic surface (LCMS) of NCSX is an important parameter that will determine the temperature profile of the SOL plasma. Design choices under consideration now could have a dramatic effect on the magnitude of L_c. If L_c is too short, the temperature profile along the field lines could be very flat with moderate to low temperature at both the target and separatrix. This could result in poor core confinement due to low edge temperature and possibly thermal instabilities at the edge due to carbon cooling. Long connection length allows a hot separatrix temperature, significant temperature drop along field lines to reasonably low target temperature, and establishment of a high recycling regime with low impurity source at the targets. Preliminary field line tracing by Grossman [13] indicates that one key to insuring long SOL field line length is to allow sufficient gap (at least 10 cm) between the LCMS and the material boundary at the tips of the bean-shaped cross sections.

11.9.3.2 Introduction

The plasma temperature at the target surface will determine the recycling regime and impurity source rate from sputtering. The temperature upstream at the LCMS is the boundary condition for the core temperature profile. Tokamak experience has shown that this separatrix temperature sets the height of the pedestal at the edge of the core plasma. Since the temperature profiles are stiff inside the tokamak core plasma, this means that the core energy content and confinement can be very sensitive to the separatrix temperature. This may also be the case in a compact, nearly axisymmetric stellarator like NCSX.

Initial field line tracing calculations with a material boundary at 4cm conformal displacement from the LCMS showed that L_c might be as short as one field period [13]. More recent computations with Li383 version 1017a2 equilibrium fields and a conformal boundary 10 cm from the LCMS indicate that L_c may be much longer [13].

The purpose of this section is to present the implications of either short or long connection length on SOL temperature (separatrix and target) and thereby raise awareness of the possible effect these two regimes could have on core confinement, impurity source and neutral hydrogen source.

11.9.3.3 Basic Equations of 1D SOL Parallel Transport

Following Stangeby [14] we look for solutions to the temperature profile in a SOL flux tube assuming parallel heat conduction dominates over convection. This has been shown to be a good assumption for the dominant electron channel in tokamaks except under detachment conditions in which the temperature is very low (~1 eV) and the density is high (~1×10^{20} m^{-3}). For non-detached SOL in NCSX, the Spitzer heat conductivity equation in the direction $s_{||}$ along the magnetic field from the LCMS to the wall is

$$d[q_{||}] / ds_{||} = d[-K_0 T^{5/2} (dT / ds_{||})] / ds_{||} = P\, G(s_{||}) / A_{||} \qquad (11.9\text{-}1)$$

where for a pure hydrogen plasma $K_{0e} \sim 2000$, $K_{0i} \sim 60$, T in [eV], and $s_{||}$ in [m]. The power from the core into the SOL is denoted as P, $G(s_{||})$ is a shape function whose $s_{||}$ integral gives unity, and $A_{||}$ is the area of the flux tube perpendicular to **B**. Thus, $q_{||} = P/A_{||}$ for $A_{||}$ constant. For $T_e \sim T_i$, electron conduction dominates the parallel energy transport in the SOL, and at sufficient collisionality, the ion power is coupled through the electron channel via energy exchange collisions.

Assuming that the power enters the flux tube at only the upstream end (outer midplane where $s_{||} = 0$) or is uniformly distributed along the flux tube only introduces a simple parameter α into the solution; $\alpha = 1$ for a localized source of $G(s_{||}) = \delta(s_{||})$ and $\alpha = 1/2$ for $G = 1/L_c$ [13]. Integrating the heat conduction equation thus gives the temperature at any point along the flux tube, $T_e(s_{||})$, in terms of either the upstream temperature, T_{eu}:

$$T_e(s_{||}) = [\, T_{eu}^{7/2} - (7\alpha/2)\, (P/A_{||})\, (s_{||}/K_{0e})\,]^{2/7}. \qquad (11.9\text{-}2)$$

Or, in terms of the target temperature, T_{et}

$$T_e(s_{||}) = [\, T_{et}^{7/2} + (7\alpha/2)\, (P/A_{||})\, (\{L_c - s_{||}\}/K_{0e})\,]^{2/7}. \qquad (11.9\text{-}3)$$

For upstream temperature at least twice the target , the upstream temperature can be well approximated by

$$T_{eu} = [\, (7\alpha/2)\, (P/A_{||})\, (L_c/K_{0e})\,]^{2/7}. \qquad (11.9\text{-}4)$$

In the evaluations given below, we set $\alpha = 1/2$, corresponding to uniform power deposition along the flux tube, but the solution does not depend very sensitively on it.

If one assumes that the sheath is the only heat sink in the SOL flux tube, *i.e.* , there are no substantial radiation losses along the tube, and that parallel pressure balance holds owing to negligible cross-field transport of parallel momentum, then stagnant flow upstream and Mach=1 flow at the target allows one to express T_{et} in terms of power and upstream density, n_u, as

$$T_{et} = (m_i/2e)\, (2q_{||}/\gamma e n_u)^2\, (7\alpha q_{||} L_c/2K_{0e})^{-4/7} \propto q_{||}^{10/7}\, n_u^{-2}\, L_c^{-4/7}. \qquad (11.9\text{-}5)$$

Here, $q_{||} = P/A_{||}$, and γ is the sum of energy sheath transmission factors for ions and electrons.

While Eq. (11.9-5) is useful for understanding the scaling trends when $T_{eu} > T_{et}$, the results presented in the examples below use the more general Eq. (11.9-3) rather than Eq. (11.9-4), so the specialized relations in (11.9-4) and (11.9-5) do not hold if $T_{eu} \approx T_{et}$. The generalized form of Eq. (11.9-5) for the target temperature is

$$T_{et} = (m_i/2e)\,(2q_{||}/\gamma e n_u T_{eu})^2 \quad (11.9\text{-}6)$$

which is solved numerically for T_{et} using Eq. (11.9-3) evaluated at $s_{||} = 0$.

11.9.3.4 NCSX Examples

For estimating the NCSX target and upstream temperatures we use K_{0e}=2000, $\gamma = 7$ and the following assumptions:

Maximum input power to the core = 12 MW
Core radiation fraction = 0.2
Power entering the SOL = 12 x 0.8 = 9.6 MW
SOL power scale width, $\lambda_{q\perp} = 2$ cm
Effective Major and minor radii, $R_{eff} = 1.4$ m, $a_{eff} = 0.28$ m
$A_{||}(SOL) = 4\pi R\ \lambda_{q\perp}(B_\theta/B)$ (extra factor of 2 accounts for two ends)
$(B_\theta/B) \sim 0.13$ for $iota_{edge} \sim 0.65$

This leaves L_c, n_u, the ion species and the injected power as parameters. Note also that the target temperature in Eq. (11.9-5) scales as the SOL power scale width, $\lambda_{q\perp}$ to the -10/7 power, through $q_{||}^{10/7}$, so this is an important unknown parameter for NCSX. In the examples below we have used $\lambda_{q\perp} = 2$ cm as inferred from measurements on W7-AS [9].

11.9.3.5 Target and Separatrix Temperatures vs. L_c and P_{inj}:

Initial results from Grossman indicated that if the material boundary was 4 cm from the LCMS up near the tips of the bean cross section then the field lines within 1 cm of the LCMS at the midplane would strike the wall within one field period. In this case, $L_c \sim 5$m. More recent results with 10 cm conformal gap between the LCMS and the wall including at the bean tips showed that the field lines very near the LCMS might remain inside the boundary for over 100 toroidal transits, $L_c \sim 1000$ m. The field line length was reduced sharply for field lines starting at the midplane farther out radially. The target and separatrix temperatures as functions of injected power are plotted for $L_c = 5$ m and $L_c = 100$ m in Figures 11-15 and 11-16 respectively.

To achieve low target sputtering and a high recycling regime in tokamaks one usually tries to minimize the plasma temperature near the targets while keeping the plasma from detaching. This means T_{et} in the range of 10-20 eV. From Figure 11-15 this low target temperature is reached in a deuterium plasma for the short L_c case only at very low input power, $P_{inj} \sim 1$ - 2 MW. Figure 11-16 then shows that the upstream temperature will be about 30 - 40 eV. Higher input power raises the upstream temperature but the target temperature also increases. For the full 12 MW case in NCSX the separatrix and target temperatures are almost equal. At low separatrix density (3e19 m^{-3}) the target temperature is much too high for considerations of plate sputtering and at higher separatrix density (6e19 m^{-3}) the separatrix temperature is too low for good core confinement (see sections below).

Long connection length , $L_c \sim 100$ m, allows substantial temperature drop in the SOL flux tube as shown in Figures 11-16 and 11-17. At the high input power of 10 MW, deuterium solutions with $T_{et} \sim 20$ eV and $T_{sep} \sim 120$ eV are possible at separatrix density of 6e19 m-3

(Figure 11-16). Even at lower density, 3e19 m-3, solutions with T_{et} ~30 eV and T_{sep} > 100 eV are possible with 5 MW of input power (Figure 11-17).

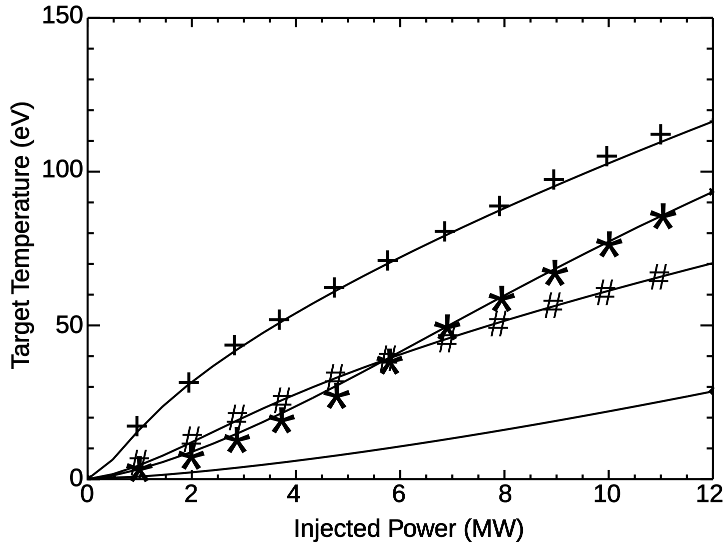

Figure 11-16. Target temperature vs injected power for four deuterium plasma cases: (a) (+) symbols use L_c = 5 m, n_u = 3.e19, (b) (#) symbols use L_c = 5 m, n_u = 6.e19, (c) (*) symbols use L_c = 100 m, n_u = 3.e19 and (d) plain line uses L_c =100m, n_u =6 e19

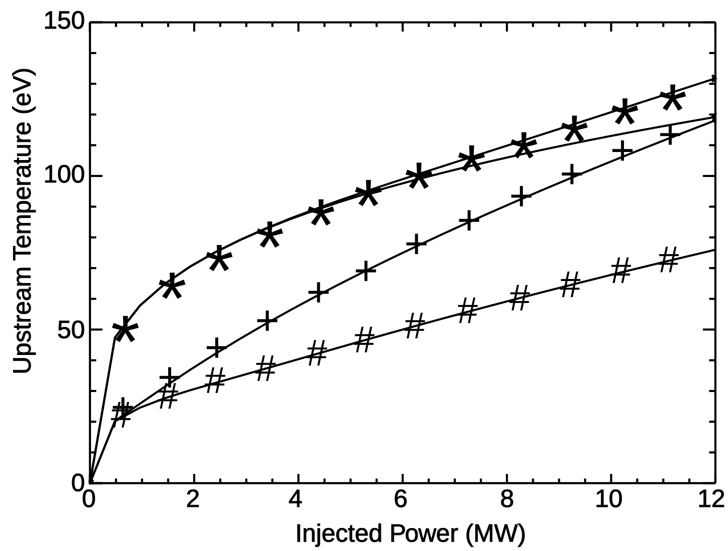

Figure 11-17. Upstream temperature vs injected power for four deuterium plasma cases: (a) (+) symbols use L_c = 5 m, n_u = 3.e19, (b) (#) symbols use L_c = 5 m, n_u = 6.e19, (c) (*) symbols use L_c = 100 m, n_u = 3.e19 and (d) plain line uses L_c =100m, n_u =6 e19

11.9.3.6 Implications of Short vs. Long Connection Length

Separatrix T_e in the 40 eV range with carbon impurity can lead to thermal instability. The carbon cooling curve increases sharply with decreasing T_e from 40 eV down to about 7 eV (see Figure11-18).

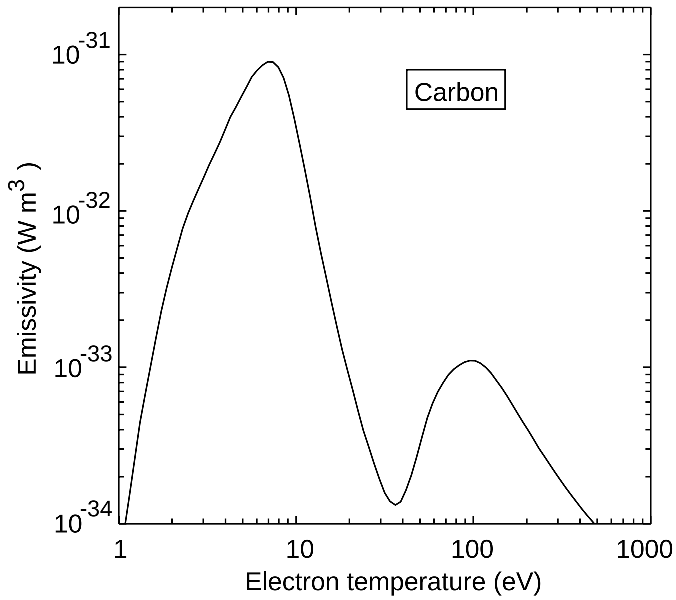

Figure 11-18. Carbon emissivity (ε) vs. electron temperature showing emissivity increase with decreasing temperature in the range $7 < T_e < 40$ eV. Radiated power is $\varepsilon n_e n_c$

If this instability occurs around the LCMS the expected result is a high density, low temperature mantle which is strongly radiating at the edge of the core plasma. If the temperature profile of the core plasma is stiff, as it is in tokamaks, then low separatrix temperature will produce low core confinement.

In diverted tokamaks the effect of this carbon thermal instability is observed in experiments with heavy gas injection to high density [15]. As the density in the SOL increases the temperature drops and the carbon radiation in the SOL increases somewhat with no appreciable decrease in core confinement. However, when the temperature at the separatrix is reduced to about 40 eV, the carbon radiation is observed to move rapidly inside the separatrix and the core confinement is reduced by a factor of two.

Long connection length allows a substantial temperature difference to be established between upstream separatrix temperature and target temperature. The separatrix temperature can be consistent with good core confinement while at the same time the target temperature can be consistent with low physical sputtering of carbon targets. The physical sputtering curve for deuterium on carbon is given in Ref. 2, p. 119. For the long L_c solution at P_{inj} = 6 MW and n_u = 5e19, T_{et} ~ 10 eV and the carbon sputtering is a factor of three less than would be the case with short L_c and T_{et} ~ 40-60 eV.

Another advantage of long connection length is that most of the temperature drop occurs near the target (see Ref. 14 p.190 cf. for discussion) so the core plasma is screened from incoming neutrals by ionization in the hot plasma not far from the target. This leads to high recycling conditions near the target at moderate core density and can even lead to detachment and substantial reduction of the heat flux on the target at higher core density.

Strong temperature gradients near the target can lead to transport of impurities away from the targets by the ∇T_i force. However the high recycling solution typically also generates sufficient flow toward the targets that the drag force on impurities balances the ∇T_i force and impurities are reasonably well entrained near the target surface. Shaping of structures in the vicinity of the targets can help to entrain the impurities.

11.9.3.7 Ideas for Achieving Long L_c

The basic tool for calculating L_c is the field line tracing code suite (VMEC, MFBE, Gourdon code) used by Art Grossman. If these calculations continue to show that field lines tend to wander radially as they transit toroidally and poloidally then a purely conformal material boundary is not the optimum for achieving long connection length. One approach would be to try to extend the material boundary outward in specified toroidal and poloidal locations where the field lines move radially outward. Present calculations indicate that most of the stretching of the material boundary should be done in the bean tips region. Depending on the engineering design this might necessitate re-optimization of the coil set somewhat to accommodate a non-conformal first wall.

11.9.3.8 Conclusions:

A two-point model of 1D energy transport in the SOL of a magnetically confined plasma has shown that for NCSX parameters, a connection length of order 5 m is insufficient to produce the desired high separatrix temperature and low target temperature needed for good core confinement and low target impurity sputtering. A connection length of order 100m would be sufficient to produce large temperature drop along SOL flux tubes from separatrix to target. Long connection length may be achievable in the NCSX design by selected perturbations of the material wall boundary away from a conformal shape about the LCMS. In particular, field line tracing calculations to date indicate that extension of the boundary farther away for the LCMS in the banana tip regions could produce the desired connection length.

11.10 Vacuum Requirements and Wall Conditioning

11.10.1 Torus Vacuum Pumping Requirements

NCSX requires sufficient wall conditioning and pumping speed to achieve base pressures of at least 2-3 x 10^{-8} torr and to recover from discharges sufficiently to allow about a 5 minute discharge repetition rate. The legacy Turbomolecular Pumping system (TMP) from PBX-M consisting of four Leybold Heraeus, 1500 l/s pumps is available for NCSX. This pumping system, together with Ti gettering, was used on the unbakeable PDX, PBX, and PBX-M vessel to achieve base pressures of ~2-3 x10^{-8} torr, and was able to recover vessel pressures from plasma discharges sufficiently rapidly to allow 3 to 5 minute discharge repetition rates, in spite of extensive internal hardware. The present plan is to mount a TMP on each of the high conductance NBI Transition Ducts, thus the application of this TMP system to NCSX will involve pump duct conductances comparable to or possibly greater than those encountered on

PBX-M. In addition, if 100 Kl/s LHe Cryopumping capability is restored to the front end of each Neutral Beamline as planned, NCSX will have considerable extra pumping speed. After the initial pumping of atmospheric components is completed, the remaining partial pressure contributions will come mainly from H_2O, CO, CO_2 and hydrocarbons. The planned NCSX Bakeout, Glow Discharge Cleaning (GDC), and Boronization capability will greatly accelerate the cleanup of these impurities.

11.10.2 Vessel Bakeout

There is considerable agreement in the international fusion community regarding the desirability of baking fusion devices with graphite plasma facing components to about 350°C as the first step toward achieving optimum wall conditions. The physics basis for baking graphite to 350°C is discussed extensively in the ITER Report prepared from the draft titled "Considerations for Bakeout and Conditioning Specifications for In-vessel Components in ITER" prepared by D. Post, ITER JCT, Jan. 20, 1995 Revised May 2, 1995. This report lists the conditioning experience of major tokamaks. The final report was reviewed by the contributors from the major tokamaks. Their interesting verbatim comments/suggestions are given in the report and form a compendium of experience that will be adopted for NCSX wall conditioning.

11.10.3 Glow Discharge Cleaning

NSTX presently uses two fixed GDC anodes; other experiments (e.g., DIII-D, JT-60U) use 2 or more GDC anodes. Given uncertainties about GDC initiation and performance in the NCSX geometry, the Helium Glow Discharge Cleaning (HeGDC) design plans for 3 ports with 4.5 inch O.D. flanges equally spaced toroidally for fixed wall anodes. These anodes will be used for both GDC and gaseous boronization. The poloidal angle of these ports is not critical although symmetrical placement will facilitate monitoring and performance analysis. In addition to the anode ports, it is desirable to have 3 ports with 4.5 inch OD flanges located near to the anode ports (preferably within line-of-sight) for Pre-ionization Filaments to facilitate GDC breakdown at the actual operating pressure and voltage. On NSTX, Pre-ionization Filaments are used routinely to initiate HeGDC between discharges, and in conjunction with ECE, to initiate plasma discharges [16,17].

11.10.4 Boronization

The NCSX Boronization method should be sufficiently convenient and economical to be an operational tool that can be applied quickly and as often as required. It should also have minimal environmental, health, and safety impact when used in the NCSX Test Cell. The NCSX Boronization method could be able to use hydrogenated or deuterated boron compounds depending on subsequent plasma operations.

A suitable and effective candidate compound for NCSX boronization is Trimethylboron [$B(CH_3)_3$ or $B(CD_3)_3$] which is presently in use at PPPL on NSTX about every 3 weeks. Trimethylboron (TMB) is about a 1000 times less toxic than diborane and nonexplosive. TMB Boronization was first tested on TEXTOR where it was found to be comparable in effectiveness to Diborane and considerably safer [18]. In addition to TEXTOR, TMB Boronization has been applied extensively on COMPASS [19], Phaedrus [20], MAST [21], and NSTX [22].

The TMB Boronization procedure consists of using the regular NCSX Gas Injection and Torus Vacuum Pumping Systems. Using one Turbomolecular pump of the Torus Vacuum Pumping System, a standard HeGDC is applied for 10 min at about 4mTorr, ~450V, ~1A per each of 3 anodes. A mixture of 90% He and 10% TMB [$B(CH_3)_3$ or $B(CD_3)_3$] containing 10 grams of TMB is injected into the HeGDC until consumed (~160 minutes). This application is followed by a 2 hr HeGDC to remove the co-deposited hydrogen or deuterium from the ~ 100 nm, B/C film. In addition to the TEXTOR results which found TMB comparable to Diborane [18], work on Phaedrus with TMB [$B(CH_3)_3$], O-Carborane [$B_{10}C_2H_{12}$], and Decaborane [$B_{10}H_{14}$] found that core oxygen concentrations were lowest for TMB (B/C = 0.33). O-carborane (B/C = 5) had twice the oxygen as TMB and Decaborane (C = 0) had nearly 3 times [20].

11.10.5 Lithiumization

Lithium wall conditioning is considered an attractive future upgrade of the NCSX wall conditioning system. Lithium pellet injection has been found to significantly improve TFTR plasma performance [23,24]. This involved using a Lithium Pellet Injector with a capacity of 270 pellets to inject up to four 3 mg lithium pellets per discharge at velocities of about 500 m/sec to near-core regions. A Lithium Pellet Injector will be a useful tool for initial NCSX lithium wall conditioning studies. However, this approach has both plasma and hardware limitations. Slow injection velocities are preferred because high injection velocities cause near-core deposition and perturbation. In addition, a small pellet size and a small number of pellets per injection may be required to prevent excessive perturbation of plasma conditions. Consequently, using lithium deposition via conventional pellet injection for plasma surface conditioning can require many discharges and is inefficient; however, other pellet injection methods might avoid these difficulties [25]. At this time, the optimum lithium characteristics have not been found, and little is known about the detailed plasma surface physics and chemistry of lithium deposited on graphite limiter surfaces [26]. The ability to increase the quantity of lithium deposition while minimizing perturbations to the plasma would provide NCSX with interesting experimental and operational options. Previous experience with Low Velocity Pellet Injection into discharges [25], Lithium Effusion Oven for deposition between discharges [27] and LASER induced ablation during discharges [28] may be of interest to the NCSX Experimental Program. The planned port access will accommodate these options.

References

[1] J. Nuehrenberg et al., IAEA Conference , Wuerzburg (1992) 449.
[2] Y. Feng et al., J. Nucl. Mater. 266-269 (1999) 812.
[3] R.W.T. Koenig, et al., 14th PSI Conference, Rosenheim, May 2000.
[4] E. Strumberger et al., Nucl Fusion, **37** (1997) 19.
[5] V.D. Shafranov, L.E. Zakharov, Nucl. Fusion **12** (1972) 599.
[6] E. Strumberger, "SOL Modeling for the W7-X Ergodic Divertor Concept," Proc. 20th EPS Conf. On Controlled Fusion and Plasma Physics, Lisboa, V.**17C**, Part II (1993) 791.
[7] J. Kisslinger *et al.*, "Island Divertor for the Stellarator Wendelstein 7-X, " Proc. 21st EPS Conf. On Controlled Fusion and Plasma Physics, Montpeiller, V.**18B**, Part II (1994) 368.

[8] D.P. Stotler and C.F. F. Karney, Contrib. Plasma Phys. **34** (1994) 392.
[9] K. McCormick et al., Proc. 12th Int. Stellarator Conference, Madison 1999.
[10] R. Schneider, M. Borchardt, J. Riemann, A. Mutzke, and S. Weber, Contrib. Plasma Phys., Vol. **40** (2000) 340.
[11] Y. Feng, F. Sardei, and J. Kisslinger, J. Nucl. Mater., Vol. **266-269** (1999) 812.
[12] X. Xu, R.H. Cohen, T.D. Rognlien, and J.R. Myra, Phys. Plasmas, Vol. **7** (2000) 1951.
[13] A. Grossman, private communication, NCSX Project Meeting presentation, Jan. 2001
[14] P. C. Stangeby, "The plasma Boundary of Magnetic Fusion Devices", IoP Publishing, 2000, pp 187 cf. and pp 221 cf.
[15] T. W. Petrie et al., J. Nucl. Mater. 241-243 (1997) 639.
[16] "NSTX Filament Preionization And Glow Discharge Cleaning Systems", H. W. Kugel, et al., PPPL Report-3381, November 1999, Proc. of the 18th Symposium On Fusion Engineering, Albuquerque, NM, October 25-29, 1999 (IEEE,1999) 296.
[17] "Overview of Impurity Control and Wall Conditioning in NSTX", H. W. Kugel, et al., Proc. of the 14th Int. Conf. on Plasma Surface Interactions In Controlled Fusion Devices, May 22-26, 2000. (To be published in J. Nucl. Mtrl.)
[18] "Borontrimethyl $B(CH_3)_3$ - A Less Hazardous Substance for Boronization", J. Winter, et. al. J. Nucl. Mater. 176 &177 (1990) 486.
[19] "Boronization of Compass", H. G. Esser et al, J. Nucl. Mater., **186** (1992) 217.
[20] "Boronization Effects on Phaedrus-T Rf Operation", M. Doczy, et al., Bull. Am. Phys. Soc. **39** (7) (1994) 1631.
[21] Private Communication, S. Fielding, Culham Science Centre, May 2000.
[22] "Intial Boronization of NSTX and the Effect On Plasma Performance", H. W. Kugel, et al., Bull. Am. Phys. Soc. **45** (7) (2000) 251.
[23] D. K. Mansfield, *et al*., "Enhancement of Tokamak Fusion Test Reactor Performance by Lithium Conditioning", *Phys. Plasmas* **3**, 1892 (1996).
[24] J. A. Snipes, *et al*., "Wall Conditioning With Impurity Pellet Injection on TFTR", *J. Nucl. Mater*., 196-198 (1992) 686.
[25] H. W. Kugel, et al., "Low Velocity Boron Micro-Pellet Injector For Edge And Core Impurity Transport Measurements", Unviersity, PPPL Report No. PPPL-3306, July 1998, Proceedings of 12th Topical Conference on High-Temperature Plasma Diagnostics, Princeton, NJ, June 7-11, 1998, Rev. Sci. Instrumen. **70** (1) (1999) 493.
[26] J. Hogan, C. Bush, and C.H. Skinner, "Lithium Effects In Plasmas, Summary Of The Workshop, PPPL, 17-18 October 1996", *Nuc. Fus*., in press.
[27] H. W. Kugel, et al., "Development of Lithium Deposition Techniques for TFTR", PPPL-3270, October 1997, Proceedings of 17th IEEE/NPSS Symposium on Fusion Engineering, 6-10 October, 1997, San Diego CA.
[28] D. K. Mansfield, et al., "DOLLOP: Improved Plasma Performance Using a New Concept for Mitigating the Plasma-Wall Interaction in Fusion Devices", Bull. Am. Phys. Soc. **42**(10) (1997) 1972, and D. K. Mansfield et al., "Observations Concerning the Injection of a Lithium Aersol into the Edge of TFTR Discharges", submitted to Nucl. Fus.